Plasma Formation in Water by Picosecond and Nanosecond Nd:YAG Laser Pulses—Part II: Transmission, Scattering, and Reflection

Kester Nahen and Alfred Vogel

(Invited Paper)

***Abstract*— We investigated the transmission, scattering, and reflection of plasmas produced in water by Nd:YAG laser pulses of 6-ns and 30-ps duration. The transmission measurements comprise a large energy range at wavelengths of 1064 and 532 nm and various focusing angles between 1.7° and 22°. This parameter range covers the parameters used for intraocular microsurgery, but also allows one to assess the influence of self-focusing on plasma shielding, which is only relevant at small focusing angles. We found that most of the laser light is either absorbed or transmitted; scattering and reflection amount to only a few percent of the incident laser energy. The transmission is considerably higher for picosecond pulses than for nanosecond pulses, regardless of the focusing angle. The plasma transmission increases with decreasing focusing angle. Self-focusing, which occurs at focusing angles below 2°, leads to a further increase of transmission. The experimental results were compared with the predictions of the moving breakdown distributed shielding model. Only partial agreement could be achieved, because the model assumes a spatially and temporally constant absorption coefficient within the plasma which is not realistic. The model can, however, be used to determine the average absorption coefficient. Fits of calculated transmision curves to the experimental data at $\theta = 22°$ yielded 900 cm$^{-1} \leq \alpha \leq$ 1800 cm^{-1} for the nanosecond plasmas and 360 cm$^{-1} \leq \alpha \leq$570 cm^{-1} for the picosecond plasmas. The efficacy of plasma-mediated intraocular laser surgery is higher with 6-ns pulses than with 30-ps pulses, because with the nanosecond pulses nearly 50% of the laser pulse energy is absorbed already at threshold, whereas it is only 8% with the picosecond pulses. The small fractional energy deposition with picosecond pulses together with a low energy threshold for breakdown can, however, be useful for the generation of very fine tissue effects. Structures beyond the laser focus are two to six times more effectively shielded from laser radiation by plasmas generated with nanosecond pulses than by picosecond plasmas. The transmitted energy at equal normalized energy $\beta = E/E_{\rm th}$ is, nevertheless, always by more than a factor of eight less for picosecond pulses because of their lower energy threshold for plasma formation.**

I. Introduction

LASER-INDUCED plasma formation in water or aqueous fluids is used in various medical laser applications [1], [2] as laser lithotripsy [2], laser angioplasty [3], and intraocular microsurgery [4]–[6]. In Part I of our study [7], we investigated how the optical breakdown threshold and the size of plasmas created at superthreshold energies depend on the laser parameters. In this paper, attention is focused on the question of how much energy is deposited into the plasma, and how much is transmitted through the plasma region, scattered, or reflected. The amount of light absorbed by the plasma influences the efficacy of the surgical procedure, and the plasma transmission is relevant for potential side effects on sensitive tissue structures behind the laser focus, e.g., the retina. The light absorption and scattering by the plasma protects the region beyond the focus and has therefore been named "plasma shielding." Owing to its importance for intraocular microsurgery and laser safety, several studies on plasma shielding have been performed already [8]–[14], mostly, however, in a very limited range of laser parameters (with the exception of [14]).

We investigate the total and time-resolved transmission of the plasma, the angular distribution of the light scattered in forward direction, and the amount of light reflected by the plasma into the aperture of the focusing lens. The plasma transmission is investigated over a large energy range for 30-ps and 6-ns pulses at wavelengths of 1064 and 532 nm, and various focusing angles between 1.7° and 22°. This parameter range covers the parameters used for intraocular microsurgery, but also allows one to asses the influence of self-focusing on plasma shielding, which is only relevant at small focusing angles.

A direct investigation of plasma absorption would require measurements with a water-filled integrating sphere. At a wavelength of 1064 nm where the absorption coefficient of water is 0.13 cm^{-1}, such measurements are, however, difficult to perform, because no equilibrium light distribution can be achieved within the sphere. We therefore deduce the absorption A from the measurement of transmission T, scattering S, and reflection R: $A = 1 - T - S - R$.

The experimental data on the time evolution and the energy dependence of plasma transmission are compared with predictions of Docchio's "moving breakdown distributed shielding model" [12], [15], [16]. The dependence of plasma transmission on laser pulse duration, energy, and focusing angle is analyzed with the help of Kenndedy's model for the calculation of breakdown thresholds [17] and by looking at the changes of energy density within the plasma which can be deduced from measurements of the plasma length presented in [7].

Manuscript received September 16, 1996. This work was supported by the Deutsche Forschungsgemeinschaft under Grant Bi-321/2-3.

The authors are with the Medical Laser Center, D-23562 Lübeck, Germany.

Publisher Item Identifier S 1077-260X(96)09599-8.

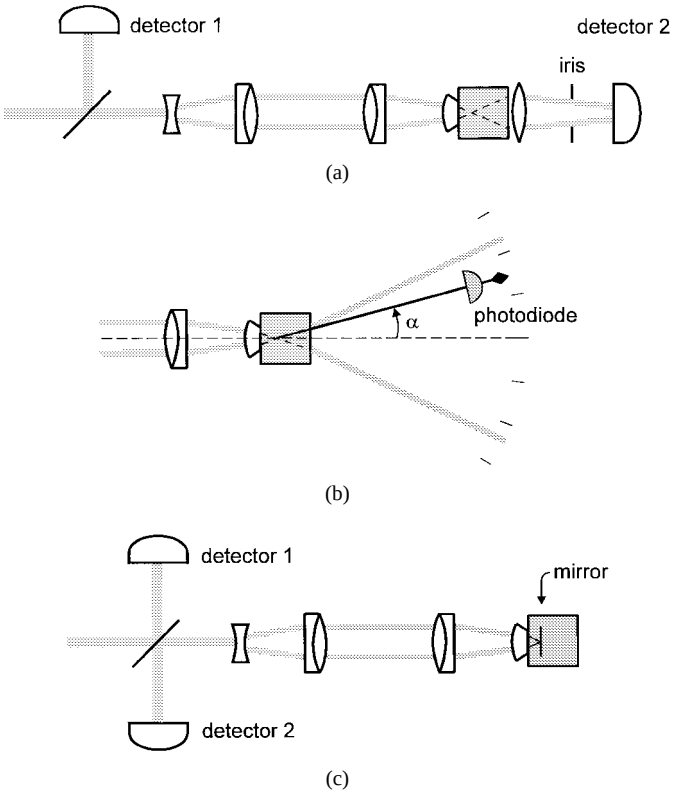

Fig. 1. Setup for the measurement of plasma transmission, scattering, and reflection. (a) Total time-integrated transmission (detector 2 = energy meter) and time-resolved transmission (detector 2 = photodiode). (b) Angular dependence of plasma transmission and scattering. (c) Back reflection into the focusing optics.

II. Methods

A. The Optical System for Plasma Generation

The plasmas were generated by focusing Nd:YAG laser pulses with durations of 6 ns and 30 ps and wavelengths of 1064 and 532 nm into a cuvette containing distilled water (Fig. 1). The delivery system of the laser pulses allowed for the realization of various focusing angles and was designed to minimize spherical aberrations. For that purpose, an ophthalmic contact lens (Rodenstock RYM) was built into the cuvette wall. A detailed description of the optical system for plasma generation and of the methods used for the measurement of the focusing angle, the spot size, and the optical breakdown thresholds can be found in part I of the study [7].

B. Measurement of Total and Time-Resolved Plasma Transmission

The total and time-resolved plasma transmission were measured with the setup depicted in Fig. 1(a). The transmitted light was focused on the detector behind the cuvette using a biconvex lens with large numerical aperture (N.A. = 0.55). For each focusing angle of the incident light, only light transmitted within that angle was collected; scattered light was rejected by an iris diaphragm. To obtain the energy $E_{\rm in}$ incident into the laser focus, the energy detector 1 (Laser Precision Rj 7100) was calibrated against a second instrument directly in front of the glass cuvette, and the measured energy values were corrected for the absorption occurring in the water between contact lens and laser focus. The transmitted energy $E_{\rm out}$ was measured with energy detector 2 (Digi Rad R-752/P-444). To account for light losses by reflections at optical surfaces and for the water absorption, detector 2 was calibrated against detector 1 assuming that far below the optical breakdown threshold 100% of the incident light would be transmitted through the laser focus. For the 6-ns pulses, 20 shots were recorded at each energy setting (pulse-to-pulse fluctuations $\pm 2\%$), and the transmission was calculated from the average of the measured energies. For the 30-ps pulses, we followed a different strategy, because the pulse-to-pulse energy fluctuations were much larger ($\pm 10\%$). A large number of $(E_{\rm in}, E_{\rm out})$ data at different energy levels were recorded and binned by a computer program into $E_{\rm in}$ intervals having a width of maximal 3% of the center value. Each interval contained at least 10 $(E_{\rm in}, E_{\rm out})$ pairs which were then used for calculating the transmission. Special attention was paid to the region of the optical breakdown threshold $E_{\rm th}$. Here, plasma formation was monitored with each shot, and transmission values with and without plasma formation were processed separately.

The time-resolved transmission was measured by means of a fast photodiode (Motorola MRD 500) with a rise time of 1.2 ns. Plasma radiation was blocked out by a filter (Schott LG 840) in front of the diode. The diode signal was recorded by a digital oscilloscope (Tektronix TDS 540) with a rise time of 0.7 ns and averaged over 1000 laser shots for each energy setting. The laser was run at only 2 Hz to largely avoid interaction between the laser pulses and residual gas bubbles from previous pulses remaining in the focal region of the laser beam.

C. Measurement of the Angular Dependence of Plasma Transmission and Scattering

Fig. 1(b) shows the experimental arrangement used for measuring the angular dependence of plasma transmission and scattering. The photodiode was moved around the plasma in steps of 2° for $\alpha \leq 10°$, and in steps of 5° for $\alpha > 10°$. The measurement range was limited by the size of the cuvette to maximally 45°. The angular resolution was 0.2°, determined by the diameter of the sensitive area of the diode (1 mm) and the distance between the diode and plasma (300 mm). The angle γ under which the light originated from the plasma was calculated from the angle α in the goniometric setup using Snell's law. The diode signal was averaged over 1000 laser shots at each measurement angle, transferred to a PC, and integrated. Measurements were performed at $\beta = E/E_{\rm th} = 0.5$ and $\beta = 15$, i.e., at energies below and 15 times above the optical breakdown threshold.

The time integrated diode signal is proportional to the energy per steradian ρ at each angle γ. The radiant energy dE transmitted into the solid angle element $d\Omega = 2\pi \sin\gamma \, d\gamma$ is thus given by

$$dE = 2\pi\rho(\gamma)\sin\gamma \, d\gamma \tag{1}$$

and the total transmitted and scattered energy is given by

$$E_{T+S} = 2\pi \int \rho(\gamma) \sin\gamma \, d\gamma. \tag{2}$$

When plasma formation occurs, the amount of the transmitted energy is reduced due to absorption, and the angular energy distribution $dE(\gamma)$ is broadened due to scattering. To assess the amount of forward scattering by the plasma at a certain value of the normalized energy β, one has to compare the angular energy distribution at this β value to the distribution it would have without plasma formation. The shape of the latter can be assessed through a measurement of the energy distribution below the breakdown threshold, for example at $\beta = 0.5$. Both curves are normalized with respect to each other using the value of the total transmission $T(\beta)$ within the focusing angle θ which is determined in a separate measurement as described above. The normalized $\tilde{\rho}(\gamma)$ and $d\tilde{E}(\gamma)$ curves must fulfil the condition

$$\frac{\int_{-\theta/2}^{\theta/2} \tilde{\rho}(\gamma)_{\mathrm{super}} \, \sin\gamma \, d\gamma}{\int_{-\theta/2}^{\theta/2} \tilde{\rho}(\gamma)_{\mathrm{sub}} \, \sin\gamma \, d\gamma} = T(\beta) \tag{3}$$

where the subscripts super and sub denote the cases with and without plasma formation.

D. Measurement of Plasma Reflection

The setup in Fig. 1(c) was used to measure the amount of light reflected by the plasma back into the cone angle of the focused laser beam. First, an aluminum mirror was placed in the laser focus and a measurement was performed at an energy where no plasma formation on the mirror occurred. In this way the calibration factor between the two energy detectors was determined for a case when about 80% of the laser light is reflected. The mirror was then removed and the plasma reflection measured for 6-ns pulses at normalized energies $3.5 \leq \beta \leq 5.5$, and for 30-ps pulses at $1.5 \leq \beta \leq 4.3$. For each measurement, the data were averaged over 100 pulses.

E. Calculation of Transmission with the "Moving Breakdown Distributed Shielding Model"

We showed in Part I of our study [7] that the plasma growth at superthreshold energies can be described by the "moving breakdown model" of plasma formation. This model, which was introduced by Ambartsumyan *et al.* [18] and Raizer [19], and later refined by Docchio *et al.* [15], describes the plasma length $z(t)$ as a function of time during a laser pulse, and the final plasma length $z_{\max}$ as a function of the dimensionless laser pulse energy $\beta = E/E_{\mathrm{th}} = I/I_{\mathrm{th}}$. Docchio extended this theory to the "moving breakdown distributed shielding model" in order to describe the time evolution of plasma transmission during the laser pulse [12], [16]. This first-order model assumes, for the sake of simplicity, a spatially and temporally constant absorption coefficient within the plasma. The transmitted laser power at time t is then determined only by the incident laser power $P(t)$ and the plasma length $z(t)$:

$$P_T(t) = P(t) e^{-\alpha z(t)}. \tag{4}$$

For a Gaussian pulse centered around $t = 0$, $P(t)$ is

$$P(t) = P_{\max} e^{-2(t/2A)^2} \tag{5}$$

whereby A is related to the laser pulse duration (FWHM) t_L by $A = t_L/2\sqrt{\ln 2}$. The plasma length $z(t)$ is given by [12], [15]

$$z(t) = \begin{cases} 0, & \text{for } t \leq t_0 \\ z_R \sqrt{\beta e^{-2(t/2A)^2} - 1}, & \text{for } t_0 \leq t \leq 0 \\ z_R \sqrt{\beta - 1}, & \text{for } t \geq 0 \end{cases} \tag{6}$$

where $z_R = \pi\omega_0^2/\lambda$ denotes the Rayleigh range and ω_0 is the focal spot radius. The plasma growth starts at the time $t_0 = t_{z=0} = -A\sqrt{2 \ln \beta}$ which depends on β. It continues until, at $t = 0$, the maximal plasma length is reached. Afterwards, the plasma length is assumed to remain constant.

The total transmission $T(\beta)$ can be obtained by calculating [12]

$$T(\beta) = \frac{\int P_T(t) \, dt}{\int P(t) \, dt} \tag{7}$$

where $P_T(t)$ and $P(t)$ are described by (4) and (5). A fit of (7) to measured $T(\beta)$ data yields the absorption coefficient of the plasma. This method of determining α considers the time evolution of the plasma length during the laser pulse and is therefore more accurate than a calculation $\alpha = z_{\max} \ln T$ based on Beer's law and the final plasma length $z_{\max}$. The latter method is easy to apply, because $z_{\max}$ can be readily obtained from plasma photographs, but it yields absorption coefficients which are too low.

III. Results and Discussion

A. Time-Resolved Plasma Transmission

Fig. 2 shows the time-resolved transmission of plasmas produced with 6-ns pulses focused at an angle of 22° for various values of β. For picosecond pulses, we could not measure $T(t)$. All curves are normalized such that the peak amplitudes of the incoming laser pulses are equal. Breakdown always starts before the maximum intensity of the laser pulse is reached. With increasing β, plasma formation starts earlier, and the area below the transmitted pulse decreases, indicating a decrease of total transmission.

B. Angular Dependence of Plasma Transmission and Scattering

Fig. 3(a) presents the angular distribution $\rho(\gamma)$ of the energy per steradian behind the laser focus with and without plasma formation for 6-ns pulses at 1064 nm. The $\rho(\gamma)$ curves were fitted through the $\rho_i(\gamma_i)$ data points measured at discrete angles γ_i. Fig. 3(b) shows the corresponding energy distributions $dE(\gamma)$ which were calculated using the fitted $\rho(\gamma)$ curves. Both distributions are given in arbitrary units, but are normalized with respect to each other according to (3). The area A below the upper curve ($\beta = 0.5$) in Fig. 3(b) corresponds to the energy incident into the focus, whereas the area below the lower curve ($\beta = 15$) corresponds to the energy

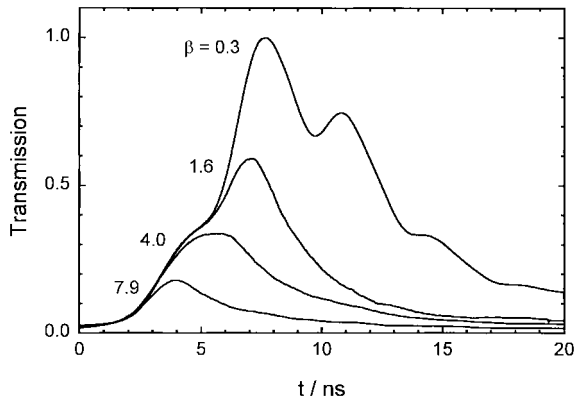

Fig. 2. Time-resolved transmission through the focal region at energies below threshold ($\beta = 0.3$) and above threshold ($\beta > 1$). All curves are averaged over 1000 laser pulses. Pulse duration 6 ns, focusing angle 22°.

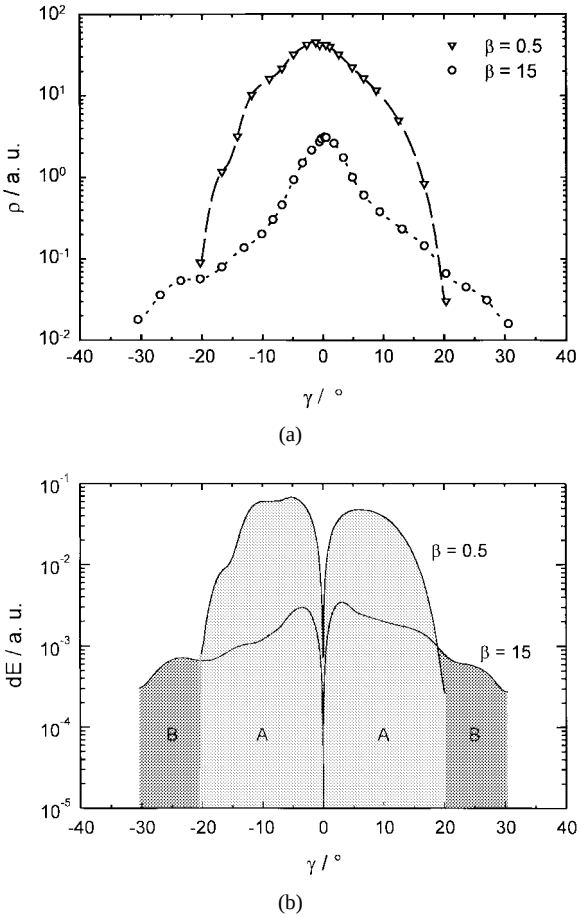

Fig. 3. Angular dependence of time-integrated plasma transmission and scattering. (a) Energy per steradian ρ plotted as a function of the angle γ between detector and optical axis. (b) Angular energy distribution $dE(\gamma)$, with $dE = 2\pi\rho(\gamma)\sin\gamma \; d\gamma$.

which is transmitted and scattered in the presence of the laser plasma. The area B represents energy of laser radiation which is scattered out of the beam in forward direction. The fraction of this radiation as compared to the incident laser energy is

$$S = \frac{B}{A}. \tag{8}$$

It has to be noted that (8) gives only a lower estimate of the scattering by the laser plasma, because light scattered at angles larger than 30° is not included. At these large angles, the irradiance was so small that no diode signal could be detected. Furthermore, some scattering may occur within the beam in directions which lie outside the e^{-2} points of the focusing angle ($\pm 11°$), but are not covered by area B.

Using (8), we obtain $S = 0.5\%$ for 6-ns pulses, and $S = 7.6\%$ for 30-ps pulses (measurement data not shown). At first sight, it seems surprising that scattering is so much stronger with picosecond pulses than with nanosecond pulses. One has to consider, however, that the transmission is also much higher: at $\beta = 15$ it is 28.4% for the 30-ps pulses and only 4.6% for the 6-ns pulses. The ratio of transmission and scattering is thus similar for both pulse durations. We find that four to nine times more light is transmitted within the cone angle of the laser beam than scattered in forward direction outside the cone angle.

Our findings agree with the results obtained by Meyerand and Haught [20] for plasma formation in argon gas. No experimental data have been reported for liquids so far.

C. Plasma Reflection

At a focusing angle of 22° and 6-ns pulse duration, the reflection back into the focusing angle was found to be 0.8 ± 0.02%, and at 30-ps pulse duration it was 1.7 ± 0.9%. No energy dependence was observed within the range investigated. Both back reflection and forward scattering are small compared to the light absorption within the plasma. The absorption is thus approximately given by $A \approx (1 - T)$. This differs from plasma formation at solid surfaces, especially at metal surfaces, where reflection plays a large role [21]–[23]. In liquids, however, the breakdown front moves toward the incoming laser beam while the light intensity of the pulse rises. The resulting plasma expansion continuously creates a new absorber with a low electron density and a small plasma frequency which is required for the incident light to be absorbed [22].

D. Total Plasma Transmission as a Function of Energy for Different Pulse Durations, Wavelengths, and Focusing Angles

1) Dependence on Pulse Duration: Figs. 4 and 5 show the energy E_{out} transmitted through the plasma and the plasma transmission T as a function of laser pulse energy for 6-ns and 30-ps pulses at a wavelength of 1064 nm and 22° focusing angle. Each figure presents the total energy range of E_{in} and an enlarged view of the threshold region. The $(E_{\text{in}}, E_{\text{out}})$ data above threshold were fitted by curves $E_{\text{out}} = a + bE_{\text{in}}^{c}$, and the same fits were then transferred into the graphs for $T(E_{\text{in}})$. The small hump at the beginning of the $(E_{\text{in}}, E_{\text{out}})$ curve of Fig. 4(a) is caused by the shoulder in the leading edge of the laser pulse (see Fig. 2). It is therefore of no general importance and was ignored for the fitting procedure. The straight lines in Figs. 4(b) and 5(b) represent 100% transmission.

The threshold behavior at both pulse durations is strikingly different: with 6-ns pulses, the transmission immediately drops to about 50% when plasma formation occurs, whereas with 30-

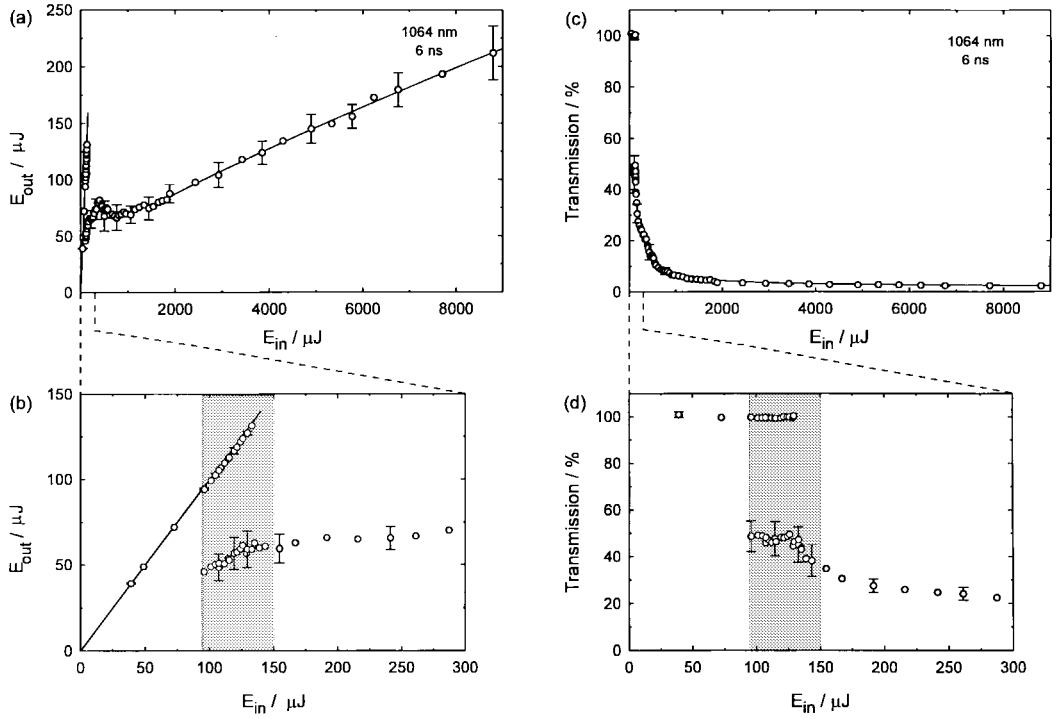

Fig. 4. (a)–(b) Transmitted energy as a function of incident energy for 6-ns pulses at a wavelength of 1064 nm and 22° focusing angle. (c)–(d) Transmission as a function of incident energy. The shaded areas in (b) and (d) indicate the threshold region between 10% and 90% breakdown probability. $E_{\rm th}$ (50% breakdown probability) lies in the center of the shaded area.

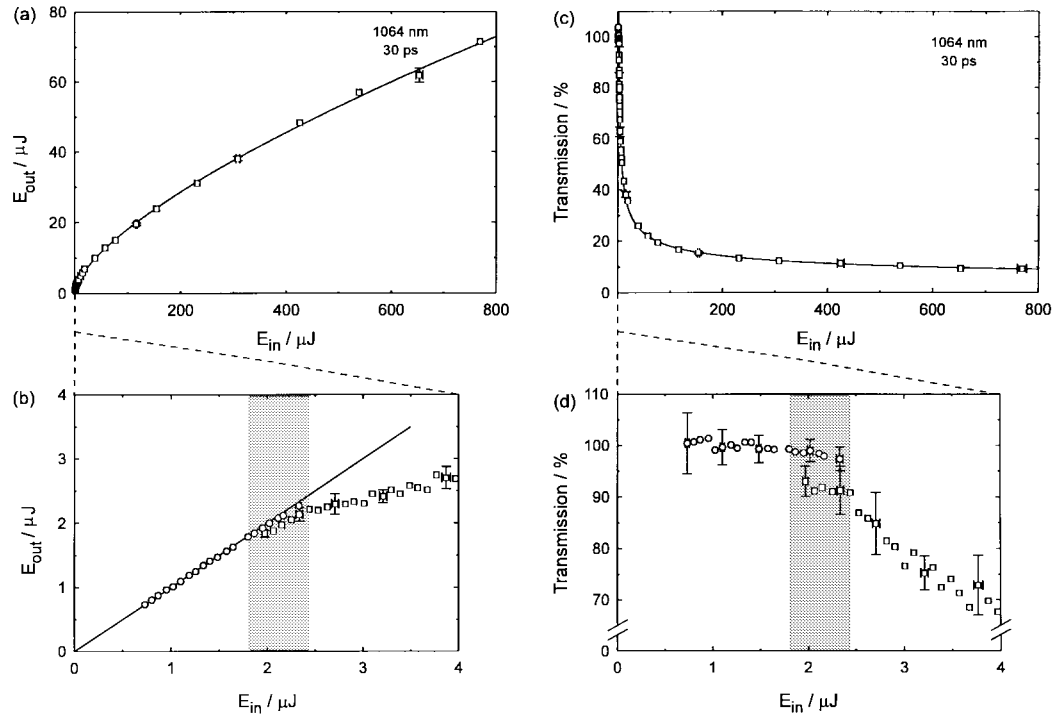

Fig. 5. (a)–(b) Transmitted energy as a function of incident energy for 30-ps pulses at a wavelength of 1064 nm and 22° focusing angle. (c)–(d) Transmission as a function of incident energy. The shaded areas in (b) and (d) indicate the threshold region between 10% and 90% breakdown probability. $E_{\rm th}$ (50% breakdown probability) lies in the center of the shaded area.

ps pulses, still more than 90% of the laser light is transmitted. Transmission is also for values well above threshold higher for the shorter pulse duration: at $\beta = 50$, the transmission is $2.8 \pm 0.2\%$ for 6-ns pulses ($E_{\rm in} = 6.1$ mJ), and $17.5 \pm 0.4\%$ for 30-ps-pulses ($E_{\rm in} = 106\ \mu$J) and even at $\beta = 300$ ($E_{\rm in} = 636\ \mu$J) the transmission for the picosecond pulses is still 9.5%. Nevertheless, the transmitted energy does not differ much when equal values of the incident energy are compared:

At $E_{\rm in} = 500\ \mu$J, for example, $E_{\rm out}$ is 68 μJ for 6-ns pulses and 52 μJ for 30-ps pulses, and at $E_{\rm in} = 800\ \mu$J, $E_{\rm out}$ is the same (70 μJ) for both pulse durations.

The different threshold behavior observed for the 6-ns and 30-ps pulses can be explained by the findings obtained in part I of our study [7] where Kennedy's model for the calculation of breakdown thresholds [17] was applied to interpret the measured threshold values. The model discriminates between a threshold I_m for the generation of seed electrons by multiphoton ionization and a threshold I_c for reaching a critical electron density $\rho_{\rm cr} = 10^{20}$ cm^{-3} by avalanche ionization. We found for both pulse durations and $\lambda = 1064$ nm that $I_m > I_c$. In this case, the measured threshold $I_{\rm th}$ is determined by I_m, and the electron density at the end of the laser pulse increases with increasing ratio I_m/I_c. The average I_m/I_c value was determined to be 45 for 6-ns pulses, but only 6 for 30-ps pulses [7]. As a consequence, a higher electron density will be reached with the nanosecond pulses. When I_m/I_c is large, the threshold irradiance can decrease during the laser pulse from I_m to a value closer to I_c, because UV radiation emitted by the already existing plasma provides initial electrons for ionization cascades occurring in the vicinity of the plasma, and the breakdown process becomes independent of the creation of initial electrons by multiphoton ionization. The reduction of the threshold during the laser pulse results in a larger plasma length as would have been achieved at a constant threshold value. This effect is, again, more pronounced for the nanosecond pulses due to the larger I_m/I_c value [7]. Both the higher electron density and the larger plasma length contribute to the higher absorption of the nanosecond plasmas.

2) Dependence on Wavelength: Figs. 6 and 7 present the transmission data for $\lambda = 532$ nm. At the shorter wavelength, the transmission of the 6-ns pulses is slightly reduced in the threshold region even when no visible plasma is formed [Fig. 6(a)]. Otherwise, the transmission is generally a little higher at 532 nm than at 1064 nm, especially well above threshold: For $\beta = 20$, the transmission is 7.4% at 532 nm as compared to 4.1% at 1064 nm for the nanosecond pulses, and 35% as compared to 25% for the picosecond pulses. Both observations can be explained considering that multiphoton absorption plays a much stronger role at the shorter wavelength. Calculations using Kennedy's model revealed that $I_m < I_c$ at 532 nm, and therefore multiphoton absorption not only provides seed electrons for the avalanche but yields a considerable contribution to the generation of free electrons throughout the whole process of plasma formation [7]. Since near threshold enough electrons are always produced by multiphoton ionization to allow avalanche ionization to occur at least to some degree, it is possible that slightly below threshold an energy density smaller than $\rho_{\rm cr}$ is reached which reduces the light transmission but does not lead to a perceivable plasma radiation. The final electron density is, on the other hand, generally not as high when $I_m < I_c$ (at 532 nm) as at 1064 nm, when $I_m \gg I_c$ and the avalanche "overshoots" the critical density $\rho_{\rm cr}$. This explains why the plasma transmission above threshold is higher at the shorter wavelength.

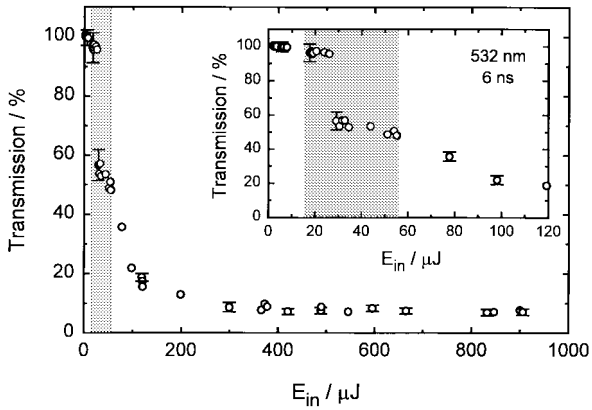

Fig. 6. Transmission as a function of incident energy for 6-ns pulses at a wavelength of 532 nm and 22° focusing angle. The insert shows the threshold region. The shaded areas mark the range between 10% and 90% breakdown probability.

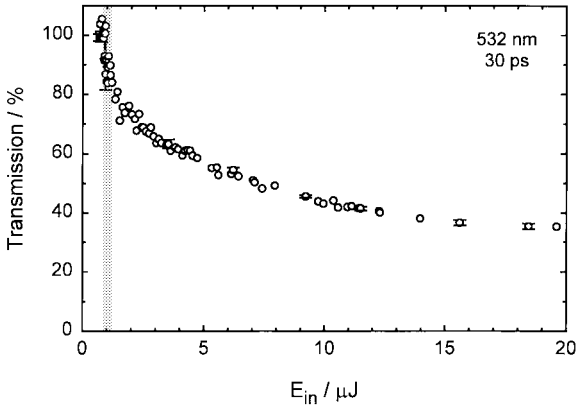

Fig. 7. Transmission as a function of incident energy for 30-ps pulses at a wavelength of 532 nm and 22° focusing angle.

3) Dependence on Focusing Angle: Figs. 8 and 9 show the dependence of transmission on the focusing angle. To facilitate a comparison between the different angles, the transmision is plotted as a function of the normalized pulse energy β. For small angles where only small β values could be investigated, the curves fitted to the measurement data are extrapolated to higher β values in order to elucidate the trends. We find that the transmission increases with decreasing focusing angle, regardless of pulse duration. This increase is most pronounced far above threshold: at $\beta = 100$, the transmission of the picosecond pulses is, for example, 2.2 times higher for an angle of 4° than for 22°.

Fig. 10 demonstrates that the transmission is even further increased at focusing angles below 2° where plasma formation goes along with self-focusing [7]. The measurements for 6-ns pulses [Fig. 10(a)] must be interpreted with some care, because they were disturbed by residual bubbles in the focal volume which did not completely disappear even with a time separation of 30 s between consecutive shots. The actual transmission is therefore higher than indicated. Continuum generation was observed for 30-ps pulses at energies above 500 μJ, but did not significantly alter transmission.

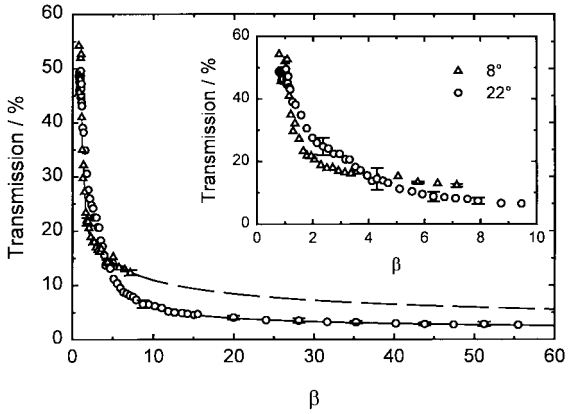

Fig. 8. Plasma transmission at various focusing angles, plotted as a function of the normalized laser pulse energy β. Pulse duration 6 ns, wavelength 1064 nm.

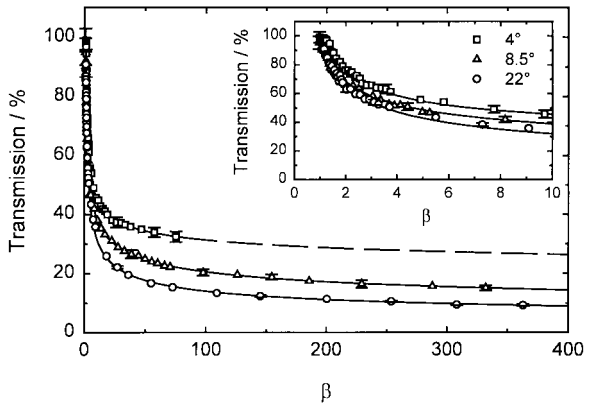

Fig. 9. Plasma transmission at various focusing angles, plotted as a function of the normalized laser pulse energy β. Pulse duration 30 ps, wavelength 1064 nm.

For picosecond pulses, the increase of transmission in the self-focusing regime can be explained by a change in the beam profile during filament formation. Self-focusing of a picosecond pulse in a Kerr liquid is a transient phenomenon, because the pulsewidth is in the order of the relaxation time of the Kerr effect [24], [25]. Therefore, the leading part of the pulse sees little induced change in the refractive index and diffracts almost linearly as it propagates in the medium. Only after some time, the induced Δn is large enough to cause beam collapse. Near threshold, where plasma formation requires beam collapse, a large part of the laser pulse will thus be transmitted through the focal region before plasma formation, and the total transmission will be high. The above explanation does not apply for nanosecond pulses where the quasi-steady-state theory of self-focusing holds [24], [25]. Nevertheless, the formation of an extended region of lower intensity around the high-intensity peak of the filament has been observed also for nanosecond pulses [24, Fig. 2], and near threshold the energy in this low-intensity region may be transmitted without leading to plasma formation. Both explanations do not hold for very large β values where plasma formation should occur also in the periphery of the beam profile. This case is, however, not covered by our study, since β was always smaller than 7 at those focusing angles where self-focusing occurred.

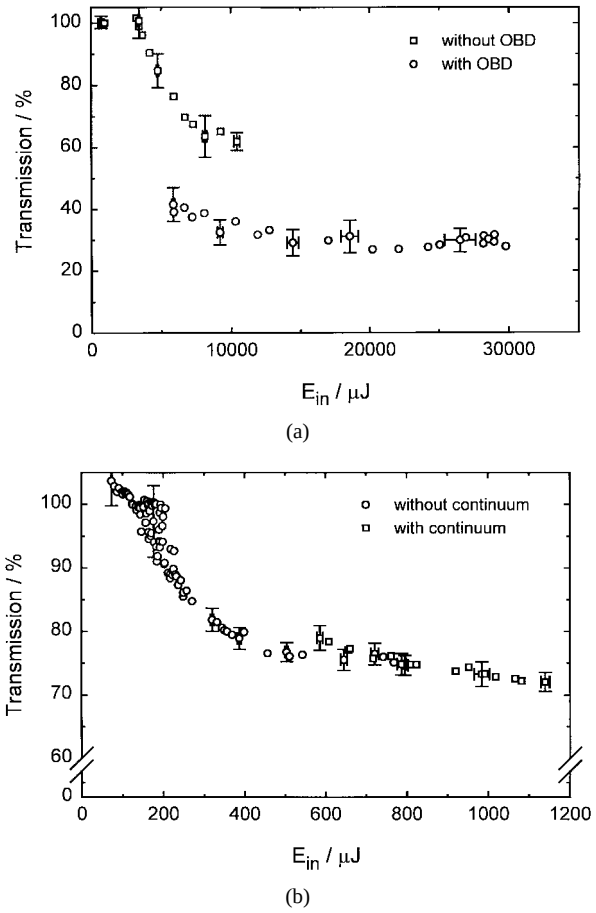

Fig. 10. Plasma transmission in the self-focusing regime, at a wavelength of 1064 nm. (a) 6-ns pulse duration, 1.8° focusing angle. (b) 30-ps pulse duration, 1.7° focusing angle.

E. Parameter Dependence of Transmission Well Above Threshold

In this section, we shall qualitatively discuss some aspects of the parameter dependence of plasma transmission well above threshold which have not yet been covered in the previous section. Since $T \approx (1 - A)$, we focus attention on the plasma absorption neglecting scattering and reflection. In the range of pulse durations investigated, absorption mainly occurs by inverse bremsstrahlung. From the requirement of energy and momentum conservation, an electron can absorb a photon by the inverse bremsstrahlung mechanism only if it is colliding with an atom, or in the field of an ion. Hence, the probability for a photon to be absorbed depends not only on the plasma length and the density ρ of free electrons, but also on the collision frequency ν between electrons and heavy particles [17], [26]. This creates a pronounced dependence of the absorption coefficient α on the energy density W within the plasma, since both ρ and ν depend on W. We shall therefore consider energy density and the plasma length $z_{\max}$ at the end of the laser pulse to interpret the parameter dependence of plasma transmission.

1) Dependence on Focusing Angle: Our experimental findings show that the transmission increases with decreasing θ. This is quite surprising at first sight, because a decreasing focusing angle goes along with a strong (approximately

quadratic) increase of the plasma length, when β is kept constant [7]. The experimental results can only be understood if the increased plasma length is compensated for by a decrease of the absorption coefficient within the plasma. This is indeed the case, because the energy density of the plasma decreases with decreasing focusing angle: at a certain energy, the plasma can grow into the cone of the laser beam until it reaches the cross section for which $I = I_{\rm th}$. This cross section is the same regardless of the focusing angle, but the distance between laser focus and the cross section is larger for smaller angles. Therefore, the volume of the cone is larger and the energy density less for smaller angles. This results in a smaller absorption coefficient compensating the larger plasma length.

2) Dependence on Pulse Energy: At large β values, the coupling coefficient $A \approx (1-T)$ of laser energy into the plasma is approximately constant, because the transmission T changes only very slowly (Figs. 8 and 9). For picosecond pulses, the plasma length $z_{\max}$ varies approximately proportional to $(\beta-1)^{1/2}$ [7], and the plasma volume is, hence, proportional to $(\beta-1)^{3/2}$ (provided that the shape of the plasma remains the same, which is the case well above threshold). These trends yield the $W(\beta)$ dependence

$$W = \frac{AE_{\rm in}}{V} \propto \frac{A\beta E_{\rm th}}{(\beta-1)^{3/2}} \approx \frac{AE_{\rm th}}{\sqrt{\beta}}, \quad \text{for} \quad \beta \gg 1. \qquad (9)$$

We obtain the remarkable result that the average energy density in the plasma decreases with increasing β. That leads to a decrease of the absorption coefficient which partly compensates for the increase in plasma length. This effect may explain why the plasma transmission remains at a fairly high level even for large β values (Fig. 9).

For nanosecond pulses focused at 22°, the plasma length is approximately proportional to $(\beta-1)^{1/3}$ [7]. Following the same line of reasoning as above, we find that $W \approx \text{constant}$ and, therefore, also $\alpha \approx \text{constant}$ when β is varied. This leads to a pronounced decrease of transmission with increasing β because of the increasing plasma length. For nanosecond pulses focused at 8°, however, we found $z_{\max} \propto (\beta-1)^{0.45}$ [7], similar to the energy dependence observed with picosecond pulses. Correspondingly, the transmission remains at a relatively high level when β increases, although near threshold it has dropped even below the values measured for $\theta = 22°$ (Fig. 8).

F. Comparison with the Moving Breakdown Distributed Shielding Model

Fig. 11 presents $T(\beta)$ curves for 6-ns and 30-ps pulses based on the moving breakdown distributed shielding model which were calculated using (7). The curves were fitted to the measurement values in the threshold region by adjusting the absorption coefficient α. A diffraction-limited spot size was used for the calculations to represent the focusing angle of 22°. The model yields an unrealistic value of 100% transmission for $\beta = 1$, because the predicted plasma length $z_{\max} = z_R(\beta-1)^{1/2}$ is zero at this β value. Reasonable transmission values can be expected only for $\beta \geq 2$, where the model predicts a plasma length $z_{\max} \geq z_R$. The fits shown in Fig. 11 were done, therefore, for a β range $2 < \beta < 5$. We obtained

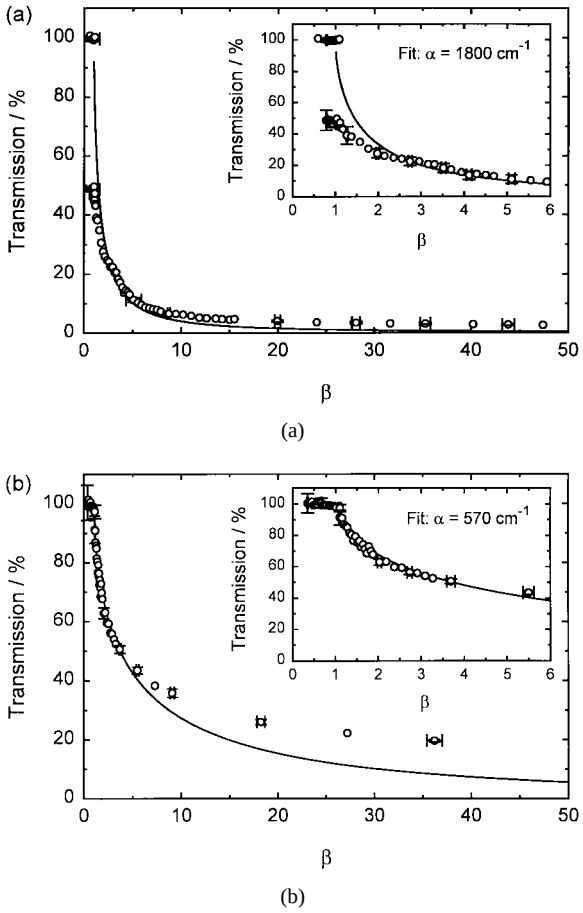

Fig. 11. Transmission $T(\beta)$ calculated using the moving breakdown distributed shielding model. The calculated curves were fitted to the experimental data for β values $2 < \beta < 5$. (a) 6-ns pulse duration, $\lambda = 1064$ nm, $\theta = 22°, \omega_0 = 1.74$ μm. (b) 30-ps pulse duration, $\lambda = 1064$ nm, $\theta = 22°, \omega_0 = 1.74$ μm. The absorption coefficients for the fits were $\alpha = 1800$ cm^{-1} for the nanosecond pulse, and $\alpha = 570$ cm^{-1} for the picosecond pulse.

$\alpha = 1800$ cm^{-1} for the 6-ns pulses at 1064 nm and 22° focusing angle, and $\alpha = 570$ cm^{-1} for the 30-ps pulses at the same parameters. Since the fits are reasonably good only for small β values, curves were fitted also for a β range $20 < \beta < 50$. In this case, we obtained $\alpha = 900$ cm^{-1} for the nanosecond pulses, and $\alpha = 360$ cm^{-1} for the picosecond pulses.

The absorption coefficient obtained for picosecond pulses is probably quite realistic, because the plasma length predicted by the model agrees well with the measured data [7]. The actual absorption coefficient for nanosecond pulses is, however, most likely not as large as calculated by the model. For equal β values, the model predicts the same plasma length for nanosecond and picosecond pulses, because it assumes a time-invariant breakdown threshold [15]. In fact, nanosecond plasmas are longer than picosecond plasmas at equal β, probably due to a decrease of the threshold during the laser pulse. They can thus produce the measured transmission with a smaller absorption coefficient than calculated.

When the $T(\beta)$ curves are fitted to the experimental data in the threshold region as done in Fig. 11, the calculated transmission values far above threshold are considerably smaller than the measured values. This is partly due to the fact that

the model assumes a homogeneous absorption everywhere within the cone angle and no light (i.e., no transmission) outside the cone angle of the laser beam. In reality, however, a certain percentage of the transmitted light passes the focus in the periphery of the laser beam where no plasma is formed (see Fig. 3). This percentage becomes probably larger with increasing β, and therefore the discrepancy between calculated and measured values increases. Another factor contributing to the discrepancy is the decrease of the average absorption coefficient with increasing β due to the decreasing energy density in the plasma which has been discussed in the previous section. Both factors contribute also to the lower α values obtained with fits of $T(\beta)$ curves to the data for $20 < \beta < 50$.

Fig. 12 shows $P_T(t)$ curves for the transmitted laser light which were calculated using the plasma absorption coefficients for the threshold region obtained from the fits in Fig. 11. The transmitted pulse shapes are calculated for various values of β. The curves are normalized by the maximum amplitude of the incoming pulse. Since the absorption coefficient of the plasma is higher for nanosecond pulses than for picosecond pulses, the transmission decreases sharply during the nanosecond pulse and more slowly during the picosecond pulse. The calculated pulse shapes for nanosecond pulses agree generally fairly well with the measured shapes of Fig. 2. They show, however, a more rapid drop of transmission when plasma formation starts than the experimental curves, because the model assumes the breakdown to occur instantaneously after the irradiance threshold is surpassed. Actually, the ionization avalanche takes some time (i.e., α increases with time), and therefore the measured curves are smoother. The second half of the calculated curve is simply an attenuated replica of the incident laser pulse, due to the model assumption of a time-invariant absorption coefficient. The measured pulse form indicates, however, that the absorption increases even after the peak power of the laser pulse has been reached. For some time after $P_{\max}$ is reached, the energy deposited into the plasma may still raise the electron density at the side of the incoming laser beam faster than it can be reduced by recombination processes. That raises the local absorption coefficient and may thus lead to an increased rate of total absorption (even if the absorption coefficient near the laser focus decreases already due to recombination processes and the beginning plasma expansion [12], [16]). This interpretation is confirmed by the fact that nanosecond plasmas are brightest at the side proximal to the laser [7, Figs. 5 and 6].

The accuracy of the moving breakdown distributed shielding model suffers from the assumptions of a spatially and temporally constant absorption coefficient of the plasma, a time-invariant breakdown threshold, and a plasma length $z_{\max} = 0$ for $\beta = 1$. The model is, nevertheless, useful for a determination of *average* values of the absorption coefficient by simply measuring $T(\beta)$.

G. Comparison to Other Authors

Besides pulse duration, wavelength, and self-focusing, the transmission also depends on the degree of optical aberrations in the delivery system: aberrations tend to considerably

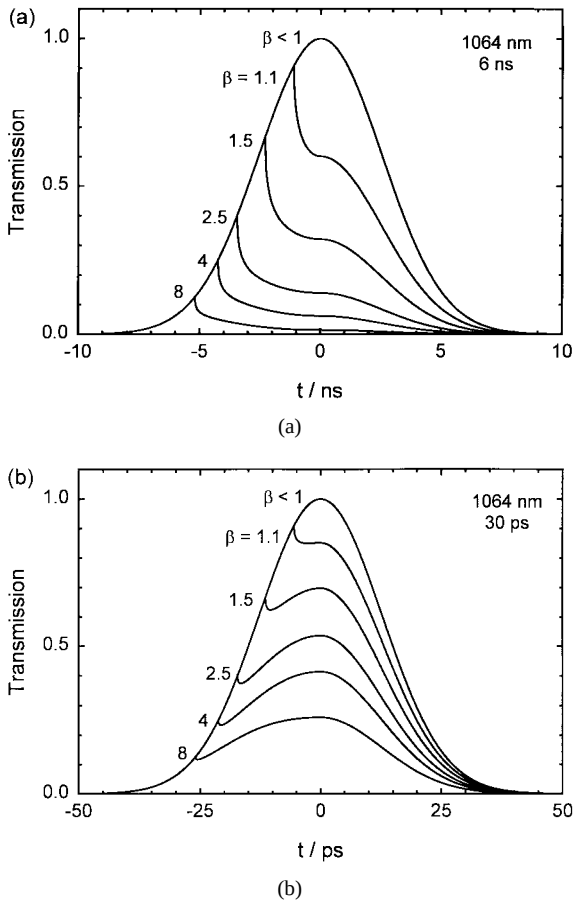

Fig. 12. Transmitted pulse shapes $P_T(t)$ for various β values, calculated by means of the moving breakdown distributed shielding model. (a) 6-ns pulse duration, $\lambda = 1064$ nm, $\theta = 22^\circ$, $\omega_0 = 1.74\ \mu$m, $\alpha = 1800\ \text{cm}^{-1}$. (b) 30-ps pulse duration, $\lambda = 1064$ nm, $\theta = 22^\circ$, $\omega_0 = 1.74\ \mu$m, $\alpha = 570\ \text{cm}^{-1}$.

increase transmission [2]. The multiparameter dependence makes a comparison of the results of different studies very cumbersome and sometimes impossible, because many relevant parameters are often not given by the authors. The most profound investigations of plasma shielding with single pulses of different duration have been performed by Docchio and Sacchi [10], and Hammer *et al.* [14]. Our observation that the transmission increases with decreasing pulse duration agrees with the findings of the second group, but disagrees with the results of Docchio and Sacchi who reported that shielding is more effective for 30-ps pulses than for 7-ns pulses. We have no conclusive explanation for this discrepancy. It should be mentioned, however, that Docchio and Sacchi's experiments were restricted to energy values near threshold, and that neither focusing angle nor spot size are given by the authors. For a discussion of the results of other authors [8], [9], [11], [13], the reader is referred to [14].

A determination of the absorption coefficient of the plasma was previously only attempted by Docchio [12]. He obtained an absorption coefficient of 70 cm^{-1} when he fitted $T(\beta)$ curves to measurement data obtained with 12-ns pulses at $\lambda = 1064$ nm and 16° cone angle in an energy range of $\beta \leq 4$ [12]. The large difference to our result (900–1800 cm^{-1} for $\theta = 22^\circ$) is probably due to three reasons: first, Docchio did not separately record the transmission for pulses with and without

plasma formation, but averaged over all measurements. This results in values for plasma transmission near threshold which are too high. Secondly, the measured spot size ($2\omega_0 = 13\ \mu$m) was 2.7 times as large as the diffraction-limited spot size, whereas in our experiments (for a slightly larger angle) it was 2.2 times as large. Docchio's measurements were thus more strongly influenced by aberrations which also tend to increase transmission [2]. Third, and very important: Docchio used the measured spot size for his calculations whereas we used the diffraction-limited spot size. Use of the measured spot size is adequate at threshold where the plasma length is not much larger than the Rayleigh range. However, it becomes more and more inadequate for increasing β, because it represents a focusing angle which, in Docchio's case, is 2.7 times smaller than the actual angle. Since the plasma length increases strongly with decreasing focusing angle, the absorption coefficients calculated for $\beta > 1$ are thus too small.

IV. Summary and Conclusion

We investigated the transmission T, scattering S, and reflection R of plasmas produced in water by Nd:YAG laser pulses of 6-ns and 30-ps duration. We found that scattering and reflection amount to only a few percent of the incident laser energy. As a consequence, the plasma absorption can be approximated by $A \approx (1 - T)$. The plasma reflection is low, because the breakdown front moves toward the incoming laser beam during the laser pulse [7], [15]. The increase of the irradiance thus leads to a creation of new plasma in front of the earlier produced plasma. This new plasma has a small electron density providing favorable conditions for light absorption, and its shielding limits the electron density which can be reached in the bulk of plasma.

The transmission is considerably higher for picosecond pulses than for nanosecond pulses, regardless of focusing angle. With 6-ns pulses, the transmission at threshold drops to 50% for all focusing angles investigated ($\theta = 5.4°$, 8°, 22°), and decreases to 3% at normalized energies larger than $\beta = 50$ (for $\theta = 22°$). With 30-ps pulses, the transmission at threshold is still 91% for focusing angles of 8.5° and 22°, and 98% for a focusing angle of 4°. At $\beta = 50$, it decreases to only 17.5% for $\theta = 22°$, 34% for $\theta = 8.5°$, and 42% for $\theta = 4°$. The difference in plasma transmission for nanosecond and picosecond pulses can be explained by the difference of the threshold values for the creation of seed electrons by multiphoton ionization (I_m) and for the completion of the ionization cascade during the laser pulse (I_c) which were obtained using Kennedy's model for the calculation of breakdown thresholds [7], [17]. Since I_m/I_c is larger for nanosecond pulses, the cascade ionization proceeds faster relative to the laser pulse duration. At the same time, the radiant energy threshold for breakdown is considerably higher for nanosecond pulses than for picosecond pulses. Both factors result in a higher electron density and, correspondingly, a larger absorption coefficient for nanosecond pulses. The larger ratio I_m/I_c is also most likely the reason why nanosecond plasmas are longer than picosecond plasmas at equal β which further reduces the plasma transmission.

The plasma transmission increases with decreasing focusing angle, most likely due to a decrease of the energy density within the plasma at lower focusing angles. Self-focusing, which occurs at very small focusing angles below 2°, leads to a further increase of transmission. This phenomenon is probably caused by changes in the beam profile leading to wings with subthreshold irradiance surrounding the high-irradiance filament where plasma is formed [24].

The experimental results were compared with the predictions of the moving breakdown distributed shielding model. Only partial agreement could be achieved, because the model assumes a spatially and temporally constant absorption coefficient within the plasma which is not realistic. The model can, however, be used to determine the average absorption coefficient. Fits of calculated transmision curves to the experimental data at $\theta = 22°$ yielded 900 cm$^{-1} \leq \alpha \leq$ 1800 cm^{-1} for the nanosecond plasmas and 360 cm$^{-1} \leq \alpha \leq$ 570 cm^{-1} for the picosecond plasmas. This corresponds to a sharp decrease of transmission during the nanosecond pulse and a smoother decrease during the picosecond pulse. The actual difference of the absorption coefficients is not as large as calculated by the model, because it assumes that nanosecond plasmas have the same length as picosecond plasmas at equal β, whereas in fact nanosecond plasmas are longer. They can thus produce the measured transmission with a smaller absorption coefficient than calculated.

A. Clinical Consequences

The efficacy of plasma-mediated intraocular laser surgery is higher with 6-ns pulses than with 30-ps pulses, because with the nanosecond pulses nearly 50% of the laser pulse energy is absorbed already at threshold. With the picosecond pulses, an absorption of 50% is achieved only at $\beta = 6$, and at threshold the absorption is less than 8%. The small energy deposition together with a low energy threshold for breakdown can be useful for the generation of very fine tissue effects down to a cellular level [27], [28], but as well it can impair effective surgery at energies near the breakdown threshold. An example is vitreoretinal surgery in the periphery of the fundus. Here, where the focus is deteriorated by aberrations because of the oblique passage of the light through cornea and lens, the breakdown threshold is strongly elevated [2], and no tissue effects could be achieved with pulse energies of up to 400 μJ [29]. Since higher pulse energies bear a high risk of retinal damage by the light transmitted through the focus, it is questionable whether vitreoretinal picosecond laser surgery close to the retina can be successful in more than a few selected cases.

Plasma shielding of structures beyond the laser focus is two to six times more effective for nanosecond pulses than for picosecond pulses. The transmitted energy at equal β is, nevertheless, always by more than a factor of eight less for picosecond pulses because of their lower energy threshold for plasma formation. Self-focusing is not relevant for intraocular microsurgery at the pulse durations investigated, because it only occurs at very small focusing angles. At shorter pulse durations, however, it will occur at larger angles and may

play a deleterious role for retinal structures, because besides narrowing the laser beam it increases the transmission through the focal region.

ACKNOWLEDGMENT

The authors appreciate helpful discussions with J. Noack and P. Kennedy.

REFERENCES

[1] S. J. Gitomer and R. D. Jones, "Laser-produced plasmas in medicine," *IEEE Trans. Plasma Sci.*, vol. 19, pp. 1209–1219, 1991.
[2] A. Vogel, "Non-linear absorption: Intraocular microsurgery and laser lithotripsy," *Phys. Med. Biol.*, vol. 42, pp. 1–18, 1997
[3] M. R. Prince, G. M. LaMuraglia, P. Teng, T. F. Deutsch, and R. R. Anderson, "Preferential ablation of calcified arterial plaque with laser-induced plasmas,"*IEEE J. Quantum Electron.*, vol. QE-23, pp. 1783–1786, 1987.
[4] R. F. Steinert and C. A. Puliafito, *The Nd:YAG Laser in Ophthalmology*. Philadelphia, PA: Saunders, 1985.
[5] F. Fankhauser and S. Kwasniewska, "Neodymium:yttrium-aluminum-garnet laser," in *Ophthalmic Lasers*, F. A. L'Esperance, Ed., 3rd. ed. St. Louis, MO: Mosby, 1989, pp. 781–886.
[6] A. Vogel, P. Schweiger, A. Frieser, M. Asiyo, and R. Birngruber, "Intraocular Nd:YAG laser surgery: Light-tissue interaction, damage range, and reduction of collateral effects," *IEEE J. Quantum Electron.*, vol. 26, pp. 2240–2260, 1990.
[7] A. Vogel, K. Nahen, and D. Theisen, "Plasma formation in water by picosecond and nanosecond Nd:YAG laser pulses: Part I—Optical breakdown at threshold and superthreshold irradiance," this issue, pp. 847–860.
[8] R. F. Steinert and C. A. Puliafito, "Plasma formation and shielding by three ophthalmic neodymium-YAG lasers," *Amer. J. Ophthalmol.*, vol. 96, pp. 427–434, 1983.
[9] R. F. Steinert, C. A. Puliafito, and C. Kittrell, "Plasma shielding by Q-switched and mode-locked Nd:YAG lasers," *Ophthalmology*, vol. 90, pp. 1003–1006, 1983.
[10] F. Docchio and C. A. Sacchi, "Shielding properties of laser-induced plasmas in ocular media irradiated by single Nd:YAG pulses of different durations," *Invest. Ophthalmol. Vis. Sci.*, vol. 29, pp. 437–443, 1988.
[11] M. R. C. Capon, F. Docchio, and J. Mellerio, "Nd:YAG laser photodisruption: an experimental investigation on shielding and multiple plasma formation," *Graefe's Arch. Clin. Exp. Ophthalmol.*, vol. 226, pp. 362–366, 1988.
[12] F. Docchio, "Spatial and temporal dynamics of light attenuation and transmission by plasmas induced in liquids by nanosecond Nd:YAG laser pulses," *Nouvo Cimento*, vol. 13, pp. 87–98, 1991.
[13] S. A. Boppart, C. A. Toth, W. P. Roach, and B. A. Rockwell, "Shielding effectiveness of femtosecond laser-induced plasmas in ultrapure water," in *SPIE Proc.* vol. 1882, pp. 347–354, 1993.
[14] D. X. Hammer, R. J. Thomas, B. A. Rockwell, E. D. Jansen, A. J. Welch, G. D. Noojin, M. Frenz, J. Noack, and A. Vogel, "Shielding properties of laser-induced breakdown in water for pulse durations from 5 ns to 125 fs," *Appl. Opt.*, submitted for publication.
[15] F. Docchio, P. Regondi, M. R. C. Capon, and J. Mellerio, "Study of the temporal and spatial dynamics of plasmas induced in liquids by nanosecond Nd:YAG laser pulses. 1: Analysis of the plasma starting times," *Appl. Opt.*, vol. 27, pp. 3661–3668, 1988.
[16] ———, "Study of the temporal and spatial dynamics of plasmas induced in liquids by nanosecond Nd:YAG laser pulses. 2: Plasma luminescence and shielding," *Appl. Opt.*, vol. 27, pp. 3669–3674, 1988.
[17] P. K. Kennedy, "A first-order model for computation of laser-induced breakdown thresholds in ocular and aqueous media: Part I—Theory," *IEEE J. Quantum Electron.*, vol. 31, pp. 2241–2249, 1995.
[18] R. V. Ambartsumyan, N. G. Basov, V. A. Boiko, V. S. Zuev, O. N. Krokhin, P. G. Kryukov, Yu. V. Senatskii, and Yu. Yu. Stoilov, "Heating of matter by focused laser radiation," *Sov. Phys. JETP*, vol. 21, pp. 1061–1064, 1965.
[19] Yu. P. Raizer, "Breakdown and heating of gases under the influence of a laser beam," *Sov. Phys. Usp.*, vol. 8, pp. 650–673, 1966.
[20] R. G. Meyerandt and A. F. Haught, "Optical-energy absorption and high-density plasma production," *Phys. Rev. Lett.*, vol. 13, pp. 7–9, 1964.
[21] J. F. Ready, *Effects of High Power Laser Radiation*. Orlando, FL: Academic, 1971.
[22] T. P. Hughes, *Plasmas and Laser Light*. Bristol: Adam Hilger, 1975.
[23] R. P. Godwin, "Multilayer optics provides laser-plasma-coupling insight," *Appl. Opt.*, vol. 34, pp. 572–580, 1995.
[24] M. M. T. Loy and Y. R. Shen, "Study of self-focusing and small-scale filaments of light in nonlinear media," *IEEE J. Quantum Electron.*, vol. QE-9, pp. 409–422, 1973.
[25] Y. R. Shen, "Self-focusing: Experimental," *Prog. Quantum Electron.*, vol 4, pp. 1–34, 1975.
[26] Y. R. Shen, *The Principles of Nonlinear Optics*. New York: Wiley, 1984, pp. 528–539.
[27] A. Vogel, M. R. C. Capon, M. N. Asiyo-Vogel, and R. Birngruber, "Intraocular photodisruption with picosecond and nanosecond laser pulses: Tissue effects in cornea, lens and retina," *Invest. Ophthalmol. Vis. Sci.*, vol. 35, pp. 3032–3044, 1994.
[28] A. Vogel, S. Busch, and U. Parlitz, "Shock wave emission and cavitaion bubble generation by picosecond and nanosecond optical breakdown in water," *J. Acoust. Soc. Amer.*, vol. 100, pp. 148–165. 1996.
[29] J. Roider, K. Nahen, and A. Vogel, unpublished observations.

Kester Nahen, for photograph and biography, see this issue, p. 860.

Alfred Vogel, for photograph and biography, see this issue, p. 860.